ChemComm

COMMUNICATION

View Article Online
View Journal | View Issue

Check for updates

Cite this: *Chem. Commun.*, 2025, **61**, 19104

Received 3rd September 2025,
Accepted 23rd October 2025

DOI: 10.1039/d5cc05082k

rsc.li/chemcomm

Open Access Article. Published on 24 October 2025. Downloaded on 6/2/2026 11:02:17 AM.
This article is licensed under a Creative Commons Attribution 3.0 Unported Licence.

Equilibrium molecular structure of cyclic(alkyl)(amino)carbene copper(I) carbazolide with intramolecular agostic and anagostic C–H···Cu interactions from gas-phase electron diffraction

Alexander V. Belyakov,[a] Nadezhda S. Kormil'tsyna,[a] Ekaterina P. Altova,[b] Pavel Yu. Sharanov,[b] Igor F. Shishkov*[b] and Alexander S. Romanov*[c]

The first gas-phase electron diffraction structure of a "carbene–metal–amide" (CMA) complex has been characterised. Strong agostic and weak anagostic C–H···Cu intramolecular interactions have been revealed and correlated with significant bending of the geometry around the copper atom, corroborated by photoluminescence in the gas phase.

The emerging organic light-emitting diode (OLED) technology is enabling advanced and next-generation display and lighting devices, including virtual reality (VR) and augmented reality (AR).[1] The success of OLED technology is impossible to imagine without advancements in molecular design of the luminophore materials, which play a key role in the emitting layer of the OLED and enable its electroluminescence. carbene–metal–amide (CMA) materials have emerged as one of the brightest and stable luminophores suitable for the fabrication of energy-efficient OLEDs using solution and vapour deposition protocols.[2–7] Their straightforward and effective molecular design relies on linear coordination of a d^{10} coinage metal (Au, Ag, or Cu) with a π-donor amide and a π-acceptor carbene ligand, enabling sub-microsecond, near-unity-efficiency thermally activated delayed fluorescence (TADF) with charge-transfer (CT) character.[8] The small singlet–triplet energy gap (ΔE_{ST}), with a value often as low as 40 meV, facilitates rapid reverse intersystem crossing (rISC) with rates of up to 10^7 s^{-1}. The extent of S_1 and T_1 states mixing is governed by the spin–orbit coupling (H_{SO}) of the coinage metal and inversely proportional to ΔE_{ST}, which in turn depends on the frontier orbital overlap integral ($S_{H/L}$) between the HOMO and LUMO; a smaller overlap leads to a smaller ΔE_{ST}.[9] Of the analyzed CMAs, gold(I)-based systems currently deliver the best performance, achieving TADF lifetimes as short as 200 ns and unity photoluminescence quantum yield (PLQY).[7–9]

Copper(I)-based CMA materials offer a significant advantage due to the greater natural abundance of copper compared to gold. However, heterotypic atomic bonds formed by copper are often significantly more polarized than are those formed by gold (due to a significant difference in the electronegativity of the interacting atoms), thus requiring additional molecular design efforts to stabilize the copper-based materials for practical applications in OLEDs. Recently, Feng *et al.*[10] and Li *et al.*[11] explained that including weak C–H···M(I) (M = Cu or Au) anagostic intramolecular interactions could provide greater stability for OLED materials with promising enhancements in device operation stability. All works to date have focused exclusively on confirming such C–H···M(I) interactions in solid-state samples, while recent work from Steffen *et al.* demonstrated the impact of weak intramolecular B–F···Cu(I) interactions on the photophysical properties of the material.[12] However, the nature of these intermolecular contacts remains controversial due to the simultaneous presence of numerous intermolecular interactions and lattice forces that closely pack molecules in the crystal, dictating a geometry that may be far from the potential energy surface minimum.[3b] It was recently demonstrated in a carbene-copper-chloride complex by comparing its gas-phase electron diffraction (GED) and single-crystal X-ray diffraction structures,[13a] while only two earlier works reported gas-phase structures for other Cu(I)-containing small molecules.[13b,c]

Explicit mapping of the agostic and anagostic interactions in OLED materials is uniquely enabled by GED, which is largely limited in XRD experiments. The current work aimed to investigate first a CMA material (molecule **CMA2**, Fig. 1) structure in the gas phase, reveal the molecular geometry of intramolecular interactions in the absence of intermolecular contacts under high vacuum, and demonstrate their impact on photoluminescence.

The electron diffraction method was combined with quantum chemical calculations up to the all-electron RI-MP2/def2-QZVPP[15–17] level of theory and compared with the crystal structures determined using X-ray diffraction analysis. Mean

[a] *Saint-Petersburg State Technological Institute, 190013 Saint Petersburg, Russia*
[b] *Department of Chemistry, Moscow State University, 119992 Moscow, Russia. E-mail: igormg@mail.ru*
[c] *Department of Chemistry, The University of Manchester, Oxford Rd., Manchester, M13 9PL, UK. E-mail: alexander.romanov@manchester.ac.uk*

This journal is © The Royal Society of Chemistry 2025

Open Access Article. Published on 24 October 2025. Downloaded on 6/2/2026 11:02:17 AM.
This article is licensed under a Creative Commons Attribution 3.0 Unported Licence.

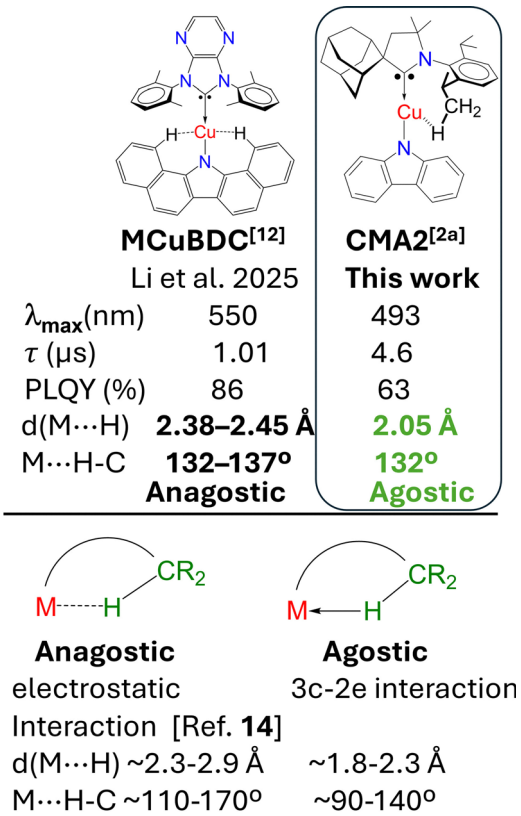

Fig. 1 Structures of CMA complexes and key photophysical parameters and structural parameters for anagostic and agostic interactions.[14]

vibrational amplitudes, $u_{ij,h1}$, and anharmonic vibrational corrections ($r_{ij,e}$–$r_{ij,a}$) were calculated for experimental temperatures, using quadratic and cubic force constants, which are required for the gas-phase electron diffraction (GED) analysis, were computed using the SHRINK program[18,19] at the first-order perturbation theory level, taking into account curvilinear kinematic effects. These calculations were carried out using Gaussian16 (Revision C01) program package.[20] A natural bond orbital (NBO-7.0)[21–23] analysis of molecule **CMA2** was performed for a wave function at the BP86BP/def2SVPP level of theory.

Molecule **CMA2** was obtained according to our previously described procedure and purified by sublimating it at 250 °C at 1×10^{-6} mbar to obtain high-purity material for the GED experiment;[2a] see SI for details. The Cartesian coordinates of its atoms were calculated according to an algorithm given in the literature.[24] For the ring closure, the calculation of the coordinates was not terminated at the last atom in the ring but continued for three dummy atoms according to the algorithm rules.[24] The problem of the ring closure was reduced to the iterative solution of nonlinear equations with respect to the dependent geometrical parameters, to have the Cartesian coordinates of dummy atoms coincide with those of the first three atoms of the ring.

$$Q = \sum_s w_s \Delta_s^2 = \sum_s w_s \left[sM^{obs}(s) - k \cdot sM^{calc}(s) \right]^2 \qquad (1)$$

Structural parameters were refined with the minimized functional having the form in eqn (1). In this equation, $s = (4\pi/\lambda)\sin(\theta/2)$ is the parameter of the scattering angle θ with λ being the wavelength of the electron beam, w_s is a weight function, $sM(s)$ is the molecular intensity function, and k is the scale factor. The value of the R-factor was taken using eqn (2) and used as a criterion of the minimum of the functional Q.

$$R = \left(Q / \sum w_s \left[sM^{obs}(s) \right]^2 \right)^{1/2} \qquad (2)$$

Least-squares structure refinements were carried out with the use of a modified version of the KCED25 program.[25] Weight matrices were diagonal. The short-distance data were taken with weights of 0.5, and the long-distance ones with unity weights. The molecular structure of the **CMA2** molecule (Fig. 1 and Fig. S1) was specified by 51 bond lengths, 154 bond angles, and 110 dihedral angles. Of them, 8 bond lengths, 30 bond angles, and 35 dihedral angles were the ring closure parameters (Table S1). Geometrical parameters and vibrational amplitudes were refined in groups with constant differences from theoretical MP2 and DFT estimates, respectively. Particularly, the mean least-square amplitudes were refined in eight groups, according to specific ranges of the radial distribution curves (Fig. 4), namely 1.0–1.2, 1.2–1.8, 1.8–2.0, 2.0–2.8, 2.8–3.2, 3.2–4.1, 4.1–5.6, and 5.6–12.0 Å. The final sM(s) and f(r) radial distribution curves are shown in Fig. 2 and 3. The correlation matrix for the set of refined geometrical parameters is given in SI. The best correspondence between the experimental and calculated molecular intensities was obtained for the final set of geometrical parameters listed in Table S1.

We compared the molecular structure of **CMA2** obtained from gas-phase electron diffraction (GED) with that from single-crystal X-ray diffraction (XRD) to elucidate the influence of intermolecular contacts on key geometrical parameters (bond lengths and angles) and on bending distortions from linear geometry. Single crystals of the **CMA2** complex were grown using a method involving slow diffusion of a layer of hexane into a CH_2Cl_2 solution.[2a] Both molecular structures of **CMA2** are shown in Fig. 4, including selected bond lengths and angles. The $C_{carbene}$–N_{amide} separation was observed to be *ca.* 0.31 Å longer in the XRD structure (3.743 Å) than in the GED structure (3.435 Å) due to both Cu–C and Cu–N bond lengths

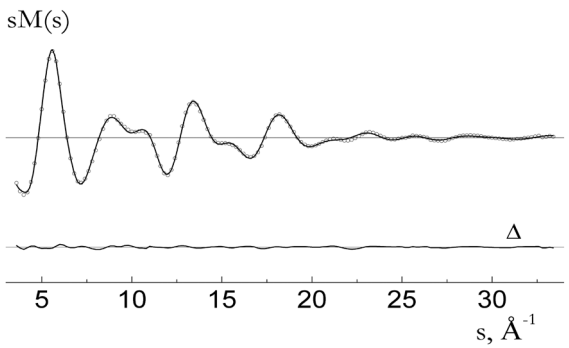

Fig. 2 Experimental (dotted) and calculated (solid) $sM(s)$ molecular intensity of **CMA2** and their difference (Δ) estimated by subtracting the theoretical values from the experimental ones.

Open Access Article. Published on 24 October 2025. Downloaded on 6/2/2026 11:02:17 AM.
This article is licensed under a Creative Commons Attribution 3.0 Unported Licence.

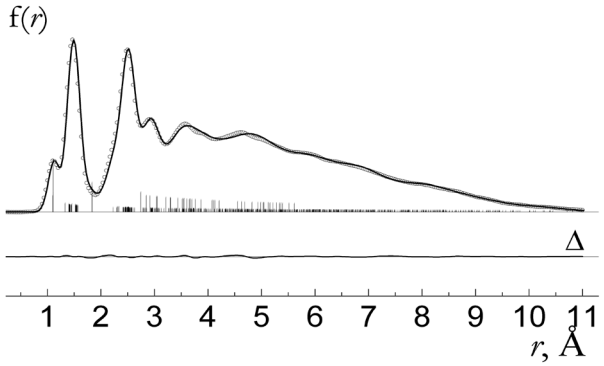

Fig. 3 Experimental (dotted) and calculated (solid) $f(r)$ radial distribution functions of molecule **CMA2** and their difference (Δ) estimated by subtracting the theoretical values from the experimental ones.

being *ca.* 0.15 Å shorter in the GED structure than in the XRD structure. The greater lengths of the covalent bonds around the copper atom in the XRD structure were attributed to the intermolecular contacts present in the crystal, for instance, weak C–H···π and C–H$^{\delta+}$(carbene)···$^{\delta+}$H–C(carbazole) interactions between neighbouring molecules, but absent for the nearly isolated molecules of **CMA2** in the gas phase. Note the shorter covalent bonds around the copper atom in the gas phase, being consistent with our earlier results for the GED structure of the carbene-copper-chloride complex (^{Me2}CAAC)-Cu(I)Cl.[13] The **CMA2** molecule was found to exhibit notable conformational distortions in the gas phase, reflected by a 23° tilt of the adamantyl moiety (Fig. 4b, top view), 18° rotation of the 2,6-diisopropylaniline-moiety along the N–C$_{carbene}$ bond (Fig. 4b, side view) and an elbow-type tilt (CMe_2 and CH_2 moieties) in the backbone of the CAAC-carbene (Fig. 4b). Rotation of the 2,6-diisopropylaniline moiety resulted in one of the methyl groups (C14) moving close to the Cu atom to form a short agostic intramolecular interaction with a Cu···H length of 2.049 Å and Cu···H–C contact angle of 132.4°. In contrast, it was observed that the methylene groups of the adamantyl moiety form short anagostic intramolecular interactions with Cu···H contact lengths of 2.305–2.391 Å and Cu···H–C contact angles of 130–131°, with these lengths significantly smaller than the sum of the van der Waals radii for Cu and H atoms (2.60 Å). Unlike the GED analysis, the XRD analysis of the **CMA2** molecule indicated only weak anagostic interactions (Fig. 4b)—with Cu···H contact distances of 2.421–2.787 Å and Cu···H–C contact angles of 135–150°,[14] values similar to those reported for **MCuBDC** complex intramolecular anagostic interactions (Fig. 1).[12]

The intramolecular interactions for **CMA2** were analyzed using Hirshfeld surface analysis,[26] to verify the presence of both agostic and anagostic Cu···H–C intramolecular interactions. This analysis indicated distinct regions of high electron density appearing between the Cu atom and C–H moieties of the carbene ligand (Fig. 4d). Further analysis of the wave function at the BP86BP/def2SVPP level of theory was performed with the quantum theory of atoms-in-molecules (QTAIM). Four Cu···H bond paths with bond critical points (3–1) were revealed and shown in Fig. S2 of the molecular graph for **CMA2**, corroborating experimental findings. The impact of short agostic Cu···H–C intramolecular contacts on the Renner-Teller distortion of the

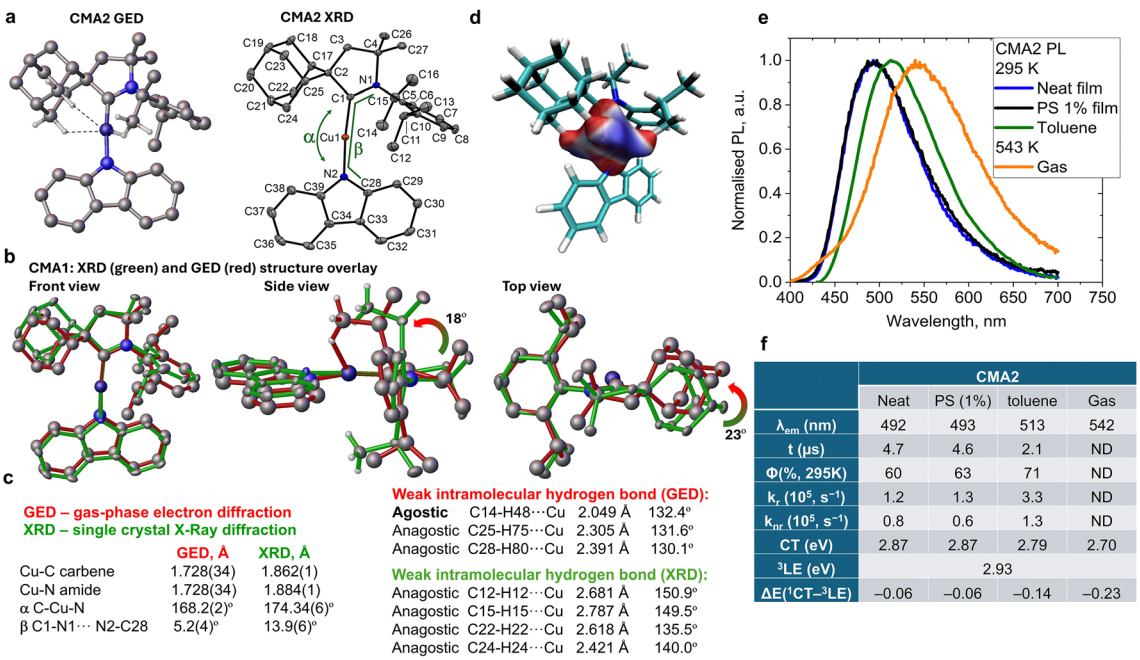

	CMA2			
	Neat	PS (1%)	toluene	Gas
λ_{em} (nm)	492	493	513	542
t (μs)	4.7	4.6	2.1	ND
Φ(%, 295K)	60	63	71	ND
k_r (10^5, s^{-1})	1.2	1.3	3.3	ND
k_{nr} (10^5, s^{-1})	0.8	0.6	1.3	ND
CT (eV)	2.87	2.87	2.79	2.70
^{3}LE (eV)	2.93			
ΔE(^{1}CT–^{3}LE)	–0.06	–0.06	–0.14	–0.23

Fig. 4 (a) Gas-phase electron diffraction (GED, showing agostic and anagostic intramolecular interactions) and single-crystal X-ray diffraction (XRD) structures for the **CMA2** molecule; (b) front, side and top views of a superposition of the GED (red) and XRD (green) structures of the **CMA2** complex (based on fitting their respective Cu, C1 and N1 atoms), demonstrating a distortion of the linear geometry around the copper center; (c) key geometrical parameters and intramolecular interactions; (d) Hirshfeld surface analysis of **CMA2**, where red corresponds to high electron density, due to formation of interactions with hydrogen atoms, while blue corresponds to low electron density with no significant interaction; (e) photoluminescence profiles for **CMA2** in various environments, where PS represents polystyrene; and (f) photophysical properties for **CMA2**, where ND represents not determined.

 This journal is © The Royal Society of Chemistry 2025

Open Access Article. Published on 24 October 2025. Downloaded on 6/2/2026 11:02:17 AM.
This article is licensed under a Creative Commons Attribution 3.0 Unported Licence.

linear geometry around the Cu atom in **CMA2** was reflected by angle α (up to 6° greater bending in the GED structure than in the XRD structure). We previously demonstrated a correlation between the tilt/twist angles in the CMA complexes and their photophysical properties.[3b] Significant bending (Renner-Teller distortion)[3b] and free rotation of the carbene aryl moiety[27] apparently resulted in up to 100 nm red shift of the photoluminescence maxima in CMA complexes, associated with the excited-state energy loss, and consistent with the non-unity PLQY observed for **CMA2**. The luminescence of gas-phase **CMA2** was measured at 543 K under high vacuum (Fig. 3 and Fig. S3), with Fig. 4f showing a comparison of the data collected in various environments to show the impact of the intramolecular agostic interaction in **CMA2**. In the gas phase, **CMA2** emits green–yellow light at a wavelength of 542 nm, which is red-shifted by up to 50 nm (1814 cm^{-1}) compared with that observed for solid-state films (492 nm) and toluene solutions (513 nm). The large Stokes shift for **CMA2** gas phase (6407 cm^{-1}) was likely linked to the presence of the short agostic interactions, providing a relaxation pathway for the excited state, and thus broadening and red shifting the emission profile compared to the solid state, having no agostic interactions.

We have demonstrated that the GED method can reveal peculiar intramolecular interactions, namely agostic and anagostic Cu···H–C intramolecular contacts, and have characterized their impact on CMA luminescence. Our results suggest the next design guidelines: CMA emitters should incorporate bulky substituents on the carbene aryl moiety to avoid agostic interactions and prevent non-radiative events. This study has shown the utility of the GED experiment for OLED-relevant large organometallics containing heavy transition-metal atoms.

A. S. R. acknowledges support from the Royal Society (grant no. URF\R1\180288, RGF\EA\181008, URF\R\231014), EPSRC (grant code EP/K039547/1 and APP46952). The work was carried out within the framework of research on the topic No. 121031300090-2 of the state assignment ''Molecular structure and supramolecular organization of individual substances, hybrid and functional materials''.

Conflicts of interest

There are no conflicts to declare.

Data availability

The data supporting this article have been included as part of the supplementary information (SI). Supplementary information is available. See DOI: **https://doi.org/10.1039/d5cc05082k**.

References

1 J. Kang, G. W. Baek, J. Y. Lee, J. Kwak and J.-H. Park, *J. Inform. Display*, 2024, **25**(3), 219–234.
2 (*a*) D. Di, A. S. Romanov, L. Yang, J. M. Richter, J. P. H. Rivett, S. Jones, T. H. Thomas, M. A. Jalebi, R. H. Friend, M. Linnolahti, M. Bochmann and D. Credgington, *Science*, 2017, **356**, 159–163; (*b*) R. Hamze, J. L. Peltier, D. Sylvinson, M. C. Jung, J. Cardenas, R. Haiges, M. Soleilhavoup, R. Jazzar, P. I. Djurovich, G. Bertrand and M. E. Thompson, *Science*, 2019, **363**, 601–606; (*c*) M. Gernert, L. Balles-Wolf, F. Kerner, U. Müller, A. Schmiedel, M. Holzapfel, C. M. Marian, J. Pflaum, C. Lambert and A. Steffen, *J. Am. Chem. Soc.*, 2020, **142**, 8897; (*d*) R. Tang, S. Xu, L. Du, F.-F. Hung, T.-L. Lam, G. Cheng, K.-H. Low, Q. Wan, S. Wu, Y. Chen and C.-M. Che, *Adv. Opt. Mater.*, 2023, **11**, 2300950; (*e*) S. Avula, B. H. Jhun, U. Jo, S. Heo, J. Y. Lee and Y. You, *Adv. Sci.*, 2024, **11**(1), 2305745; (*f*) Y. Ao, Y. Tan and S. Gong, *Adv. Opt. Mater.*, 2024, **12**, 2303333.
3 (*a*) A. S. Romanov, S. T. E. Jones, L. Yang, P. J. Conaghan, D. Di, M. Linnolahti, D. Credgington and M. Bochmann, *Adv. Opt. Mater.*, 2018, **6**(24), 1801347; (*b*) Q. Gu, F. Chotard, J. Eng, A.-P. M. Reponen, I. J. Vitorica-Yrezabal, A. W. T. Woodward, J. Penfold, D. Credgington, M. Bochmann and A. S. Romanov, *Chem. Mater.*, 2022, **34**(16), 7526–7542.
4 P. J. Conaghan, S. M. Menke, A. S. Romanov, S. T. E. Jones, A. J. Pearson, E. W. Evans, M. Bochmann, N. C. Greenham and D. Credgington, *Adv. Mater.*, 2018, **30**(35), 1802285.
5 P. J. Conaghan, C. S. B. Matthews, F. Chotard, S. T. E. Jones, N. C. Greenham, M. Bochmann, D. Credgington and A. S. Romanov, *Nat. Commun.*, 2020, **11**(1), 1758.
6 S. Shi, M. C. Jung, C. Coburn, A. Tadle, M. R. Sylvinson, D. Djurovich, P. I. Forrest and S. R. Thompson, *J. Am. Chem. Soc.*, 2019, **141**(8), 3576–3588.
7 (*a*) A. Ying and S. Gong, A Rising Star: Luminescent Carbene–Metal–Amide Complexes, *Chem. – Eur. J.*, 2023, **29**(59), e202301885; (*b*) T.-Y. Li, S.-J. Zheng, P. I. Djurovich and M. E. Thompson, *Chem. Rev.*, 2024, **124**(7), 4332–4392.
8 A. C. Brannan, H.-H. Cho, A.-P. M. Reponen, S. Gorgon, N. L. Phuoc, M. Linnolahti, N. C. Greenham and A. S. Romanov, *Adv. Mater.*, 2024, **36**, 2404357.
9 (*a*) R. Czerwieniec, M. J. Leitl, H. H. H. Homeier and H. Yersin, *Coord. Chem. Rev.*, 2016, **325**, 2–28; (*b*) C. N. Muniz, J. Schaab, A. Razgoniaev, P. I. Djurovich and M. E. Thompson, *J. Am. Chem. Soc.*, 2022, **144**(39), 17916–17928.
10 X. Feng, J.-G. Yang, J. Miao, C. Zhong, X. Yin, N. Li, C. Wu, Q. Zhang, Y. Chen, K. Li and C. Yang, *Angew. Chem., Int. Ed.*, 2022, **61**, e202209451.
11 Q. Zhang, N. Li, X. Wan, X.-F. Song, Y. Zhang, H. Liu, J. Miao, Y. Zou, C. Yang and K. Li, *Angew. Chem., Int. Ed.*, 2025, **64**, e202419290.
12 B. Hupp, J. Nitsch, T. Schmitt, R. Bertermann, K. Edkins, F. Hirsch, I. Fischer, M. Auth, A. Sperlich and A. Steffen, *Angew. Chem., Int. Ed.*, 2018, **57**, 13671–13675.
13 (*a*) A. V. Belyakov, E. P. Altova, A. N. Rykov, P. Yu. Sharanov, I. F. Shishkov and A. S. Romanov, *Molecules*, 2023, **28**(19), 6897; (*b*) A. S. Alikhanyan, K. V. Didenko, G. V. Girichev, N. I. Giricheva, O. A. Pimenov, S. A. Shlykov and G. A. Zhurko, *Struct. Chem.*, 2011, **22**(2), 401–409; (*c*) D. Hnyk, M. Bühl, P. T. Brain, H. E. Robertson and D. W. H. Rankin, *J. Am. Chem. Soc.*, 2002, **124**(27), 8078–8084.
14 (*a*) G. dos, P. Gomes, G. Xu, X. Zhu, L.-M. Chamoreau, Y. Zhang, O. Bistri-Aslanoff, S. Roland, I. V. Alabugin and M. Sollogoub, *Chem. – Eur. J.*, 2021, **27**, 8127–8142; (*b*) M. Raizada, F. Sama, M. Ashafaq, M. Shahid, M. Ahmad and Z. A. Siddiqi, *J. Mater. Chem. C*, 2017, **5**, 9315–9330.
15 F. Weigend and M. Häser, *Theor. Chem. Acc.*, 1997, **97**(1–4), 331.
16 A. Hellweg and D. Rappoport, *Phys. Chem. Chem. Phys.*, 2015, **17**(2), 1010–1017.
17 (*a*) A. Hellweg, C. Hättig, S. Höfener and W. Klopper, *Theor. Chem. Acc.*, 2007, **117**(4), 587–597; (*b*) C. Lee, W. Yang and R. G. Parr, *Phys. Rev. B: Condens. Matter Mater. Phys.*, 1988, **37**, 785–789.
18 V. A. Sipachev, *J. Mol. Struct. Theochem.*, 1985, **121**, 143.
19 V. A. Sipachev, in *Advances in molecular structure research*, ed.I. Hargittai and M. Hargittai, JAI Press, New York, 1999, 5, p. 263.
20 M. J. Frisch, *et al.*,*Gaussian 16 Rev. C.01*, Gaussian 16 Rev., Wallingford, CT, 2016.
21 F. Weinhold and C. R. Landis, *Discovering Chemistry With Natural Bond Orbitals*, John Wiley & Sons, Upper Saddle River, NJ, 2012, 300.
22 F. Weinhold and C. R. Landis, *Valency and Bonding A Natural Bond Orbital Donor-Acceptor Perspective*, Cambridge Univ. Press, Cambridge, UK; New York, 2005, 760.
23 E. D. Glendening, C. R. Landis and F. Weinhold, *J. Comput. Chem.*, 2019, **40**(25), 2234–2241.
24 R. L. Hilderbrandt, *J. Chem. Phys.*, 1969, **51**(4), 1654–1659.
25 B. Andersen, H. M. Seip, T. G. Strand and R. Stolevik, *Acta Chem. Scand.*, 1969, **23**, 3224–3228.
26 M. A. Spackman and D. Jayatilaka, *Cryst. Eng. Commun.*, 2009, **11**(1), 19.
27 C. Riley, W. Jones, N. L. Phuoc, M. Linnolahti and A. S. Romanov, *Org. Electron.*, 2025, **137**, 107156.